ECCD Studies for a Volumetric Neutron Source (VNS)

Emanuele Poli[1,*], *Mattia* Siccinio[1,2], *Alessandro* Bruschi[3], *Emiliano* Fable[1], *Thomas* Franke[1,2], and *Chuanren* Wu[4]

[1]Max-Planck-Institut für Plasmaphysik, 85748 Garching bei München, Germany
[2]EUROfusion-Consortium, 85748 Garching bei München, Germany
[3]Istituto di Scienza e Tecnologia dei Plasmi, CNR, 20125 Milano, Italy
[4]Karlsruhe Institute of Technology (KIT), 76344 Eggenstein-Leopoldshafen, Germany

Abstract. We explore the theoretical capabilities of Electron Cyclotron Current Drive (ECCD) in a volumetric neutron source (VNS), a high-neutron-fluence tokamak for component testing and qualification that is being considered in the frame of the EUROfusion Consortium. Two selected applications are addressed, namely bulk current drive in the plasma centre and stabilization of Neoclassical Tearing Modes (NTMs). It is shown that a current drive efficiency above 50 kA/MW can be reached, close to typical values reported for DEMO central ECCD. Suppression of NTMs should require less than 10 MW, but this power might become marginal in case of significant beam broadening caused by density fluctuations. The optimum launcher parameters for the envisaged applications will be further iterated to find the sweet spot between physics and engineering constraints.

1 Introduction

In the frame of the EUROfusion Consortium, both a tokamak demonstration power plant (DEMO) and a smaller tokamak for high-fluence neutron production (VNS) are being developed. The EU DEMO design focuses on a tokamak with a major radius in the range of 8 m, a central density of the order of 10^{20} m^{-3} and a central temperature around 30 keV [1, 2]. VNS (baseline 2024) is a tokamak with major radius roughly a factor of three smaller than in DEMO, higher density and lower temperatures, see Sec. 2 for more details. Its goal is to test and qualify blanket, plasma-facing components and tritium cycle in a realistic environment at large neutron fluence (expected in the range of tens of displacements per atom) but at the same time at a comparatively low tritium consumption, so that the machine does not need to rely on tritium self-sufficiency [3, 4]. In both machines, the injection of electron cyclotron (EC) waves is envisaged among other goals as an actuator for current profile control and NTM stabilization [5, 6]. This paper focuses on the results of beam tracing modelling for VNS, whose parameters are presented in Sec. 2. Some DEMO results are briefly recalled in order to provide a useful comparison. A recent summary of beam tracing calculations performed for DEMO plasmas can be found in Ref. [7]. Scanning different frequencies and injection geometries, it is found that an ECCD current well above 50 kA/MW is theoretically achievable in the centre of VNS. An estimate based on global machine parameters yields very similar results. Possible refinements of this estimate are discussed in Sec. 3. The stabilization of neoclassical tearing modes (NTMs) is addressed in Sec. 4, where again the impact of different launch conditions is analyzed, considering also beam scattering due to density fluctuations. Conclusions are drawn in Sec. 5.

2 VNS parameters

VNS is designed to operate a deuterium-tritium (DT) plasma in which fusion reactions (and hence neutrons) are generated mainly by beam-target reactions, although some fraction of the fusion power should result from thermal DT reactions. To this aim, VNS should be equipped with neutral beam injection (NBI) delivering up to 40 MW of power through the injection of 120 keV deuterium beams [8–10]. The design point employed in the present study is based on a magnetic equilibrium calculated with the free-boundary code CREATE [11, 12], from which a self-consistent plasma scenario has been generated using the transport code ASTRA [13]. The major radius is $R = 2.67$ m, the minor radius $a = 0.63$ m, the magnetic field on axis $B = 5.6$ T, the plasma current $I_p = 2.54$ MA and the effective charge $Z_{\rm eff} = 1.2$. The machine relies on a high bootstrap fraction and a significant NBI current drive to achieve steady-state plasmas. The density and temperature profiles are displayed in Fig. 1 as a function of ρ_p (square root of the normalized poloidal flux). As compared to DEMO, the targeted density is approximately twice as high (still well below the Greenwald limit [6]). On the other hand, the electron temperature drops with respect to DEMO by a factor of ca. 2/3.

The electron cyclotron current drive (ECCD) efficiency is known to scale roughly proportionally to T_e/n_eR [14]. As a consequence, the drop in the ratio T_e/n_e in VNS as compared to DEMO is nearly compensated by the re-

*Corresponding author: emanuele.poli@ipp.mpg.de

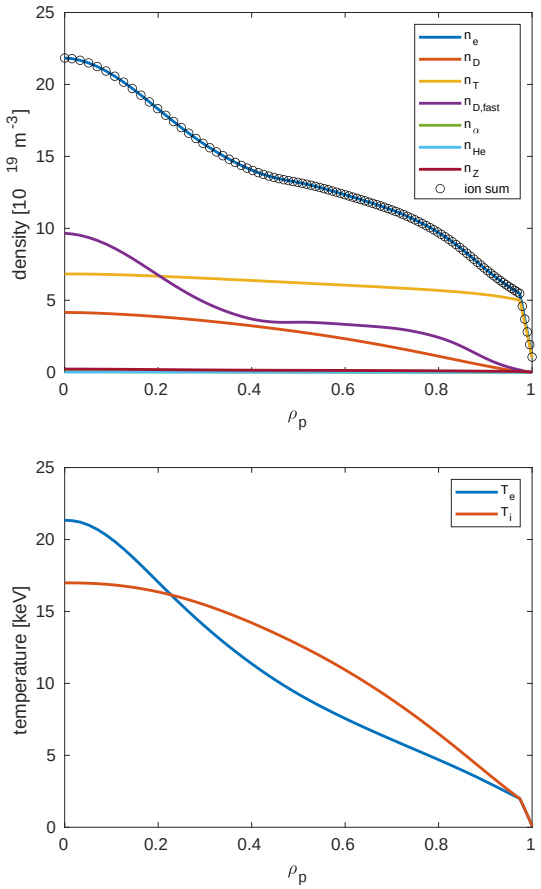

Figure 1. Density (top) and temperature (bottom) profiles employed in the VNS calculations.

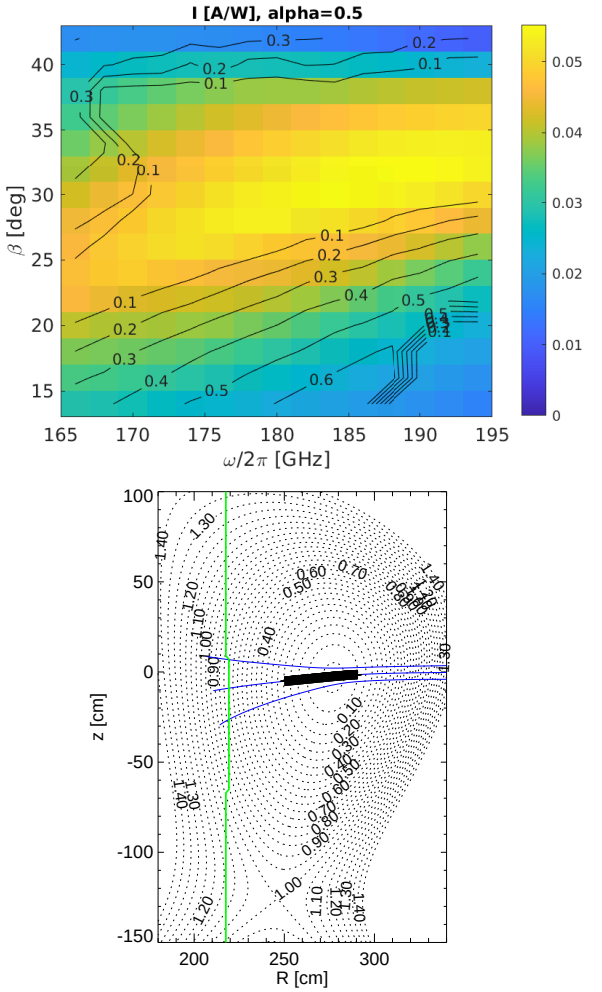

Figure 2. Achievable driven current per unit injected power in VNS for launch from $(R, Z) = (370, 0)$ cm (top) and poloidal projection of the beam propagation for the most efficient injection geometry (bottom). The black contours in the top plot represent the position of maximum absorption in terms of ρ_p.

duction of the major radius. Thus ECCD efficiencies similar to those predicted for DEMO can be expected.

For the parameters reported above, the electron cyclotron frequency on axis is $\nu_{ce} = 157$ GHz, while the electron plasma frequency on axis is $\nu_{pe} = 133$ GHz. Since for this value of the cyclotron frequency the EC heating scheme must rely on fundamental-harmonic O-mode injection, for which corresponding gyrotron sources are available, significant refraction is expected when the beam propagates close to the plasma core.

The ASTRA scenario also provides the profiles of the safety factor q and the bootstrap current density $j_{\rm bs}$. These are important for the calculation of the EC power required for the NTM stabilization. The $q = 3/2$ and $q = 2$ surfaces, assumed to be those most prone to NTMs, are located at $\rho_p = 0.55$ and $\rho_p = 0.75$, respectively. The relatively central location of these rational surfaces, as compared for instance to the $Q = 10$ ITER scenario [15], relaxes the constraints on NTM stabilization through EC waves, since the ratio T_e/n_e and hence the ECCD efficiency usually increase from the edge to the core. Moreover, a larger distance of the $q = 2$ from the wall widens the time window for NTM control before mode locking.

Presently, the VNS design assumes that the EC power is launched from an equatorial port. The performance of the EC system in terms of bulk current drive and NTM stabilization is discussed in the next two sections, where possible benefits from injection above/below the midplane are explored. The final design should result from a feedback loop between physics and engineering optimization (see e.g. Refs. [16, 17] for the ITER EC system).

3 Bulk current drive

As mentioned in Sec. 2, VNS targets steady-state discharges relying on purely non-inductive currents (NBI and bootstrap). In order to assess the design margins, it is important to know to which degree the current profile can be influenced by the injection of EC waves in the plasma core for a given allocated power. For the calculation of the EC beam propagation, absorption and current drive, the code `TORBEAM` [18] is used. The code implements a paraxial approach for the treatment of diffraction effects and assumes a linear regime for power absorption.

For the determination of the maximum achievable EC current, scans over frequency and injection angles have been performed from different launch points. In Fig. 2 (top), the ECCD current per unit injected power is shown as a function of the wave frequency $\omega/2\pi$ (x-axis) and toroidal injection angle β (y-axis). The poloidal injection angle α is fixed to 0.5° downwards. A maximum driven current of $I_{CD} = 55.2$ kA/MW is achieved injecting a 188 GHz beam with $\beta = 32°$. For these parameters, the poloidal projection of the beam path is shown by the bottom plot of Fig. 2. The green vertical line represents the position of the cold resonance, while the thicker black line along the central ray emphasizes the region where the beam is absorbed. A significant Doppler shift with respect to the cold resonance is visible. The scan over launch angles and frequencies has been repeated also for other launch positions. The results are reported in Table 1.

Table 1. Maximum achievable current from different launch points and corresponding injection angles, frequency and parallel refractive index at absorption maximum. The coordinates are given in cm, the frequencies in GHz and the driven current in kA/MW. The bottom line reports an estimate based on global parameters (`HARE` module, see text).

(R, Z)	(α, β)	freq.	I_{CD}	$N_\parallel$
$(350, 0)$	$(0.5°, 34°)$	188	55.2	0.706
$(370, 0)$	$(0.5°, 32°)$	188	55.2	0.707
$(350, 80)$	$(43°, 34°)$	191	58.6	0.704
$(330, 100)$	$(56°, 34°)$	186	59.2	0.663
`HARE`		195	59.7	0.620

Some conclusions can be drawn from this table. First of all, a current well above 50 kA/MW is found in the centre of the plasma. This confirms that current drive efficiency in the range expected for DEMO [19] can be achieved in VNS. The lower temperature and higher aspect ratio actually have the advantage of negligible parasitic second-harmonic absorption, which is often affecting the DEMO high-ECCD scenarios. Assuming as an example an available power of 10 MW, roughly 20% of the plasma current could be driven by EC waves under optimum conditions. It is also seen that a displacement of the launch point by 20 cm in the equatorial plane does not lead to any noticeable difference in the EC driven current. The maximum ECCD efficiency is achieved for a wave frequency around 190 GHz, i.e. significantly larger than the cyclotron frequency on axis. Moreover, an improvement in the driven current is obtained by moving the launch point to an elevated position. The favourable impact of injecting the wave from the top of the vessel is expected from previous theoretical analyses (see [19, 20] and references therein) and has been confirmed in experiments recently [21]. The fact that a top launch increases the driven current by less than 10% in the present analysis, while the corresponding increase in DEMO scenarios can be around 30-40% [20] (and even more if the scenario is tuned to maximize the effect [21]) is mainly due to the larger VNS aspect ratio. This increases the distance between the cyclotron harmonics and thus deceases the parasitic absorption (a problem that is exacerbated in DEMO by the higher electron temperature), and also reduces the role played by particle trapping.

In the Fisch-Boozer [22] scheme that is relevant in these applications, a large current drive efficiency is obtained if the wave power is deposited on high-energy electrons, since they have lower collisionality. This in turn requires high values of the parallel refractive index $N_\parallel$ (large Doppler shift), so that the wave-particle resonance occurs on the tail of the electron distribution function. On the other hand, in order to avoid a too large spread of the power deposition (that would occur if the absorption is too low), a sufficient number of electrons must be involved in the wave-particle interaction. This leads to the opposite requirement that the resonance should remain sufficiently close to the bulk of the distribution function. The optimum ECCD conditions result from a compromise between both trends.

These considerations have been implemented in the routine `HARE` to estimate the maximum achievable ECCD on the basis of global parameters only [19]. `HARE` is based on the fundamental assumption that it is possible to locate a "representative point" in parameter space (identified as the position of maximum absorption) at which a single evaluation of the ECCD efficiency can be performed. The efficiency itself is computed using the same routine called by `TORBEAM`, which is based on an adjoint model with momentum-conserving corrections [23, 24]. This approach relying on a single-point evaluation of the ECCD efficiency allows a fast estimate of the total driven current, which can be performed also when a detailed plasma scenario (magnetic equilibrium, kinetic profiles) is not available and ray/beam tracing scans cannot be performed. The prediction of `HARE` for the VNS scenario under consideration is reported at the bottom of Table 1. It can be seen that the maximum driven current in `HARE` matches quite well the results of the explicit optimization from `TORBEAM` scans. On the other hand, the optimum frequency predicted by `HARE` is somewhat higher than that found with `TORBEAM`, and the wavevector is smaller. Although these discrepancies are small, it is instructive to inspect them more closely.

As shown in the appendix, `HARE` predicts accurately the energy of the resonant electrons at the reference point, i.e. it reproduces the value found in the `TORBEAM` optimization. The discrepancy of ω and $N_\parallel$ between `HARE` and `TORBEAM` is not related to a different prediction of the representative point in velocity space, but rather in position. As a matter of fact, `HARE` usually employs the value of R and B at the geometric axis as an input, because these are global ("engineering") parameters that are supposed to be always available. Using as an input for R the value of the magnetic axis, $R = 2.77$ m, and estimating the magnetic field at the position of maximum absorption assuming $B \propto 1/R$, `HARE` predicts an optimum frequency $\omega/2\pi = 187$ GHz, very close to the `TORBEAM` value, also considering that the optimization scan was performed with a frequency step of 2 GHz. The optimum driven current in

HARE decreases in this case to 57.9 kA/MW, which is still very close to the TORBEAM value. The parallel wavevector does not change appreciably, but it should be remarked that the derivation of the HARE equations assumes that $N_{\|}$ is constant during the absorption process, which is only approximately valid. In any case, while the standard version of HARE already delivers a reliable estimate of the maximum EC current for VNS, this analysis suggests that including explicitly the shift of the magnetic field at maximum absorption with respect to the field at the geometric axis might improve the closeness of the HARE estimate to the reference point in parameter space obtained from a ray/beam tracing analysis.

4 NTM stabilization

The criteria that apply for the optimization of NTM control via ECCD are different from those leading to maximum EC bulk current drive discussed in the previous section. This is due to the fact that maximum current drive leads inherently to rather broad deposition profiles, while for efficient NTM stabilization the current should be driven inside the magnetic island, which advocates well-localized absorption. Here we will assume that the ECCD profile is still somewhat broader than the typical "marginal" island width at which self-stabilization occurs [25] and will employ as a simple criterion for NTM suppression [26] the formula

$$\frac{j_{\mathrm{CD}}}{j_{\mathrm{bs}}} > 1.2, \qquad (1)$$

i.e. the driven current density should exceed by 20% the (unperturbed) bootstrap current at the rational surface. Assuming that the driven current scales linearly with the injected power, Eq.(1) translates in a constraint on the minimum injected power needed for stabilization, once the current driven by 1 MW of injected power is known.

The stabilization power determined from Eq. (1) is reported in Fig. 3 for different launch conditions (position, frequency, injection angles) as a function of the toroidal launch angle beta. For injection from the midplane downwards, a stabilization power well below 10 MW is achieved by launching 140 GHz (blue diamonds) and 150 GHz (red triangles) EC beams for both the $q = 2$ and the $q = 3/2$ surface. NTM stabilization on the latter surface is generally less demanding, given the more favourable T_e/n_e ratio at smaller minor radii that leads to larger ECCD efficiencies. Further scans are shown for the $q = 2$ surface. While the power for NTM suppression increases to levels around 10 MW for injection of 160 GHz beams (green circles), it drops to ca. 8 MW for injection of 140 GHz beams from the midplane upwards (cyan triangles). To obtain the curves displayed in Fig. 3, the poloidal angle is scanned and the toroidal angle is selected in such a way that the peak of the EC current density profile is located on the desired rational surface. Two further scans show the results for a beam injected horizontally either from the midplane (dark red squares) or from an elevated location $(R, Z) = (350, 41)$ cm (magenta stars). In this case, the frequency is changed in such a way that the $q = 2$ surface is hit for a given toroidal launch angle. Horizontal

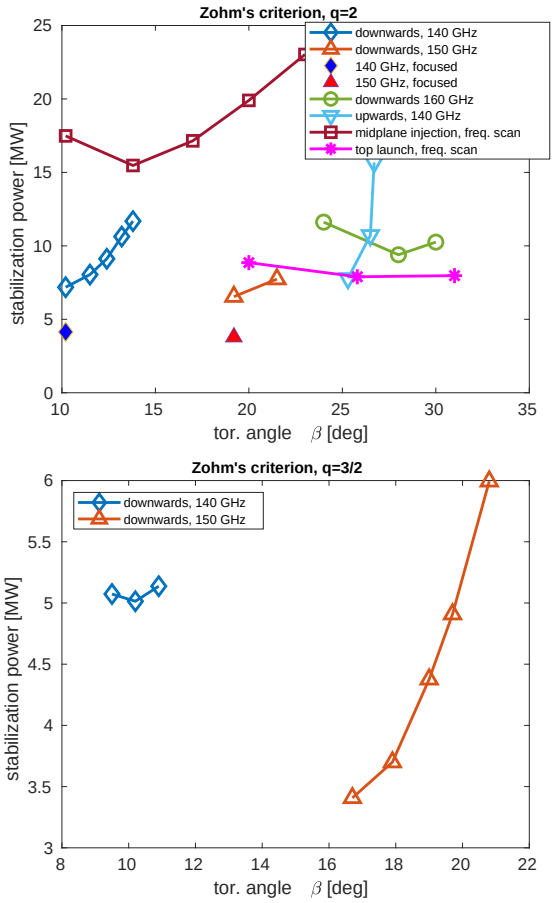

Figure 3. Power required for NTM stabilization for different launch conditions for modes developing on the $q = 2$ surface (top) and on the $q = 3/2$ surface (bottom), based on Zohm's stabilization criterion, Eq.(1).

injection in the midplane shows a rather poor stabilization performance, while the stabilization power drops again below 10 MW for horizontal launch from the top. The results described above are obtained for a Gaussian beam with a radius ($1/e$-level of the electric-field amplitude) of 4 cm and a very weak focusing (radius of curvature of the phase front of 580 cm at the launch position). The full blue diamond and the full red triangle demonstrate the potential benefit of focusing the beams onto the rational surface to reduce the deposition width (but see discussion on the role of beam scattering below). The trends shown in Fig. 3 can be explained by considering that the most efficient way to reduce the deposition width when it is dominated by the finite path of the beam through the resonance is to select the injection parameters such that the beam is tangent to the target surface. In each scan, the *total* driven current does not exhibit significant variations, and the highest current *density* corresponds as a rule to the tangency condition described above. An example of such a path is shown in the right plot of Fig. 4.

The situation in which the beam path is tangent to the rational surface, however, is also most prone to the effect of beam broadening due to scattering by density fluctuations. The impact of beam scattering, that is predicted

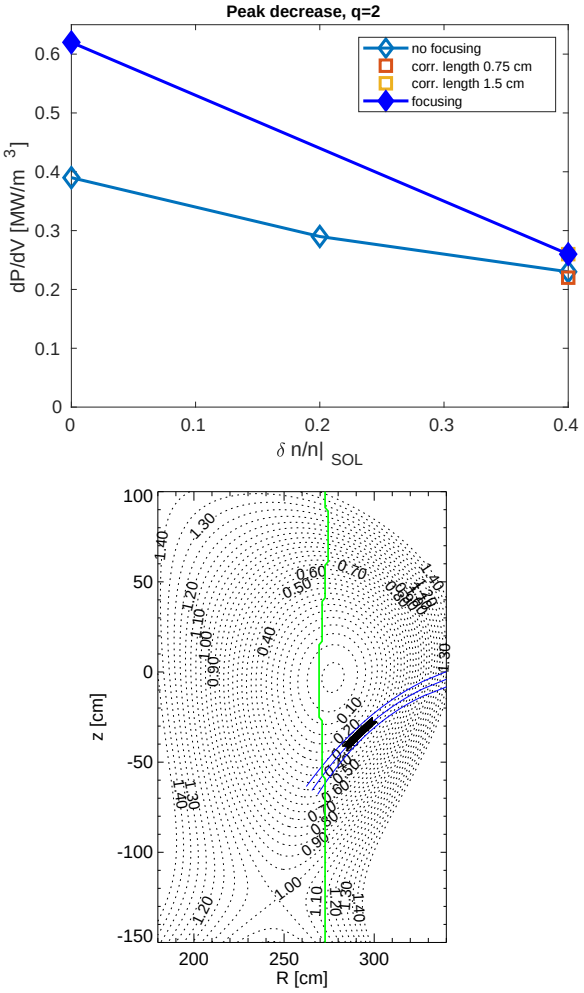

Figure 4. Top: peak power density from WKBeam simulations as a function of the relative density fluctuation amplitude. Bottom: beam path for injection of a 150 GHz beam from the midplane onto the $q = 3/2$ surface (bottommost triangle in Fig. 3, lower plot). In the top plot, open diamonds correspond to 140 GHz, unfocused beams, full diamonds to 140 GHz, focused beams, while the squares refer to simulations with different correlations lengths (unfocused beam).

to be significant in future machines like ITER [15, 27], is calculated by the wave-kinetic-equation solver WKBeam [28], which returns the statistically-averaged beam absorption in the limit of the Born approximation. Due to the aforementioned vicinity of the beam frequency to the cutoff density, it can be expected that fluctuations will play a non-negligible role also in VNS, despite its comparatively small size. While the applicability of the WKBeam approach has been confirmed through comparison to full wave codes [29] and to experimental data [30], the largest source of uncertainty for reliable predictions remains the quantification of the radial profile of the density fluctuations. Here we follow the approach discussed in [15] and adopt a profile aimed to mimic the radial dependence of $\delta n_e/n_e$ typical of H-mode plasmas: the fluctuation level is fixed to 2% the plasma core, rising linearly in the region $0.97 < \rho_p < 1$ to either 20% or 40% . As for the density correlation length, also required as an input by WKBeam, a value between 5 and 10 ρ_i is taken, where ρ_i is the ion Larmor radius calculated using the ion temperature in the pedestal. The decrease of the peak value of the absorbed power density $\mathrm{d}P/\mathrm{d}V$ caused by beam broadening with increasing fluctuation level can be seen in the top plot of Fig. 4. Since the calculation of the driven current is presently not included in WKBeam, the decrease of $\mathrm{d}P/\mathrm{d}V$ is considered as a proxy for the corresponding deterioration of the peak current drive. The launching conditions for the open blue diamonds are the same as for the bottommost open blue diamond in Fig. 3, i.e. 140 GHz, weakly focused beam, toroidal injection angle $\beta = 10.2°$. Increasing the fluctuation level from 0 to 40%, the peak value of the power density decreases by ca. 40% from 0.39 to 0.23 MW/m^3. A corresponding decrease of the driven current would lead to a stabilization power in the range of 10 MW. For comparison, the full blue diamonds in Fig. 4 correspond to the same injection conditions as for the full blue diamond of Fig. 3, i.e. including a focusing of the beam onto the $q = 2$ surface (radius of curvature of the wave front at the launch position 90 cm). While a significant gain in the peak power, corresponding to the decrease of the stabilization power shown in Fig. 3, can be appreciated when the fluctuations are turned off, the beneficial effect of focusing is almost completely spoiled at an edge fluctuation level of 40%. These results are obtained setting a correlation length of 1 cm in WKBeam. Two further simulations performed for a weakly focused beam and $\delta n_e/n_e = 40\%$ changing the correlation length to 0.75 and 1.5 cm do not exhibit any major change of the absorption profile, the peak power density remaining in the range between 0.22 and 0.26 MW/m^3 (squares in Fig. 4; the yellow square is almost entirely covered by the full blue diamond).

5 Summary and discussion

This article presents a first exploratory survey of the theoretically achievable performance of the ECCD system in the volumetric neutron source under conceptual design in the EUROfusion Consortium. It is noted that, although the predictivity of the theory cannot be tested yet in really reactor-relevant plasmas, previous comparisons between experimental measurements and linear/quasilinear predictions give a good confidence in the reliability of the underlying theoretical approach [21, 31]. A comparatively high current drive, exceeding 50 kA/MW, can be obtained with beam frequencies around 190 GHz. Injection from an elevated position leads to a modest performance increase (below 10%), which would probably not justify the corresponding technological challenges in terms of design and maintenance. This high CD efficiency adds some flexibility to the design of the machine and of the plasma scenarios, considering that the total plasma current is in the range of 2.5 MA. On the other hand, the stabilization of (2,1) NTMs might require a power of the order of 10 MW, which would be not available for other applications. This will impact the decision about the total installed EC power.

Moreover, it is remarked that the most efficient NTM stabilization is achieved for frequencies in the range of 140-150 GHz, well below the optimum frequencies for bulk current drive. While this result is in line with previous studies, it leads to the obvious question about the choice of the optimum frequency of an EC system for VNS, in case only one frequency should be selected. In order to fix this and other design parameters, further analysis involving a feedback between physics goals, launcher optical design and gyrotron technology issues will be required in the future.

Acknowledgments: This work has been carried out within the EUROfusion consortium, funded by the European Union within the Euratom Research and Training Programme (Grant Agreement No 101052200 – EUROfusion). Views and opinions expressed are however those of the author(s) only and do not necessarily reflect those of the European Union or the European Commission. Neither the European Union nor the European Commission can be held responsible for them.

Appendix A HARE equations

The optimum wave frequency ω and parallel wavevector $N_\parallel$ are calculated in HARE respectively as [19]

$$\frac{\omega}{n\Omega_a} = \sqrt{u_{\parallel-}^2 + 1} + \sqrt{u_{\parallel-}^2 \left(1 - \frac{R_a^2}{R_{pp}^2}\right)} \tag{2}$$

and

$$N_\parallel = \frac{1}{u_{\parallel-}} \left(\sqrt{u_{\parallel-}^2 + 1} - \frac{n\Omega_a}{\omega} \right). \tag{3}$$

In the previous expressions, Ω_a is the (non-relativistic) cyclotron frequency calculated at R_a, the major radius corresponding to maximum absorption, while R_{pp} refers to the position of the "pinch point", i.e. the largest value of R for which the resonance with a given harmonic is possible (dictated by the condition $n\Omega_{pp}/\omega = \sqrt{1 - N_\parallel^2}$). Finally, $u_{\parallel-}$ is the low-energy intersection of the resonance curve in velocity space with the $u_\parallel$-axis, computed at the position of maximum absorption. Here, $\mathbf{u} = \gamma\mathbf{v}/c$ is the normalized relativistic momentum. The value of $u_{\parallel-}$ is calculated from the relation $\mathcal{E} \simeq mc^2(\sqrt{u_{\parallel-}^2 + 1} - 1)$, where $\mathcal{E}$ is the energy of the resonant electrons at the position of maximum absorption.The value of $\mathcal{E}$, in turn, is determined as the maximum electron energy compatible with sufficient absorption as discussed in above in the text, see [19] for details. It turns out that $\mathcal{E}$ is estimated rather accurately in HARE, being $\mathcal{E}/T_e = 3.2$ for the present VNS scenario, to be compared to $\mathcal{E}/T_e = 3.3$ from explicit top launch optimization with $(R, Z) = (330, 100)$ cm using TORBEAM.

References

[1] G. Federici et al., The EU DEMO staged design approach in the pre-concept design phase, Fus. Eng. Des. **173**, 112959 (2021). https://doi.org/10.1016/j.fusengdes.2021.112959

[2] M. Coleman et al., Definition of an EU-DEMO design point robust to epistemic plasma physics uncertainties, Nucl. Fusion **65**, 036039 (2025). https://doi.org/10.1088/1741-4326/ada6d9

[3] G. Federici et al., Testing needs for the development and qualification of a breeding blanket for DEMO, Nucl. Fusion **63**, 125002 (2023). https://doi.org/10.1088/1741-4326/ad00cb

[4] C. Bachmann et al., Engineering concept of the VNS - a beam-driven tokamak for component testing, Fus. Eng. Des. **211**, 114796 (2025). https://doi.org/10.1016/j.fusengdes.2024.114796

[5] T. Franke et al., Integration concept of an electron cyclotron system in DEMO, Fus. Eng. Des. **168**, 112653 (2021). https://doi.org/10.1016/j.fusengdes.2021.112653

[6] M. Siccinio et al., Plasma scenario definition for a Volumetric Neutron Source (VNS) for component testing and qualification, in preparation.

[7] E. Poli et al., ECCD studies for EC-DEMO plasmas, EPJ Web of Conf. **313**, 01005 (2024). https://doi.org/10.1051/epjconf/202431301005

[8] T. Haertl et al., Vacuum pumping concept for quasi-continuous NBI operation at a steady state fusion machine, Fus. Eng. Des. **213**, 114864 (2025). https://doi.org/10.1016/j.fusengdes.2025.114864

[9] C. Hopf et al., Neutral Beam Injection for a tokamak-based Volumetric Neutron Source, Fus. Eng. Des. **213**, 114870 (2025). https:/doi.org/10.1016/j.fusengdes.2025.114870

[10] T. Franke et al., Integration studies of a positive neutral beam injector system into the design of a volumetric neutron source, Fus. Eng.Des. **215**, 115035 (2025). https://doi.org/10.1016/j.fusengdes.2025.115035

[11] R. Albanese et al., CREATE-NL+: A robust control-oriented free boundary dynamic plasma equilibrium solver, Fus. Eng. Des. **96-97**, 664 (2015). https://doi.org/10.1016/j.fusengdes.2015.06.162

[12] E. Acampora et al., Scenario feasibility and plasma controllability for Volumetric Neutron Source (VNS), Fus. Eng. Des. **217**, 115053 (2025). https://doi.org/10.1016/j.fusengdes.2015.06.162

[13] G. V. Pereverzev, P. N. Yushmanov, ASTRA: Automated System for Transport Analysis in Tokamaks, IPP 5/98, Garching: Max-Planck-Institut für Plasmaphysik (2002). https://hdl.handle.net/11858/00-001M-0000-0027-4510-D

[14] T. C. Luce et al., Generation of localized noninductive current by electron cyclotron waves on the DIII-D tokamak, Phys. Rev. Lett. **8**3, 4550 (1999). https://doi.org/10.1103/PhysRevLett.83.4550

[15] A. Snicker et al., The effect of density fluctuations on electron cyclotron beam broadening and implications

for ITER, Nucl. Fusion **58**, 016002 (2018). https://doi.org/10.1088/1741-4326/aa8d07

[16] G. Ramponi et al., Physics analysis of the ITER ECW system for optimized performance, Nucl. Fusion **48**, 054012 (2008). https://doi.org/10.1088/0029-5515/48/5/054012

[17] M. A. Henderson et al., Overview of the ITER EC upper launcher, Nucl. Fusion **48**, 054013 (2008). https://doi.org/10.1088/0029-5515/48/5/054013

[18] E. Poli et al., TORBEAM 2.0, a paraxial beam tracing code for electron-cyclotron beams in fusion plasmas for extended physics applications, Comp. Phys. Comm. **225**, 36 (2018). https://doi.org/10.1016/j.cpc.2017.12.018

[19] E. Poli et al., Fast evaluation of the current driven by electron cyclotron waves for reactor studies, Phys. Plasmas **25**, 125001 (2018). https://doi.org/10.1063/1.5050345

[20] E. Poli et al., Electron-cyclotron-current-drive efficiency in DEMO plasmas, Nucl. Fusion **53**, 013011 (2013). https://doi.org/10.1088/0029-5515/53/1/013011

[21] Xi Chen *et al.*, Doubling off-axis electron cyclotron current drive efficiency via velocity space engineering, Nucl. Fusion **62**, 054001 (2022). https://doi.org/10.1088/1741-4326/ac544a

[22] N. J. Fisch and A. H. Boozer, Creating an asymmetric plasma resistivity with waves, Phys. Rev. Lett. **45**, 720 (1980). https://doi.org/10.1103/PhysRevLett.45.720

[23] Y. R. LinLiu et al., Electron cyclotron current drive efficiency in general tokamak geometry, Phys. Plasmas **10**, 4064 (2003). https://doi.org/10.1063/1.1610472

[24] N. B. Marushchenko et al., Electron cyclotron current drive calculated for ITER conditions using different models, Nucl. Fusion **48**, 054002 (2008) and Erratum Nucl. Fusion **49**, 129801 (2009). https://doi.org/10.1088/0029-5515/48/5/054002

[25] O. Sauter et al., Marginal β-limit for neoclassical tearing modes in JET H-mode discharges, Plasma Phys. Control. Fus. **44**, 1999 (2002). https://doi.org/10.1088/0741-3335/44/9/315

[26] H. Zohm et al., Control of NTMs by ECCD on ASDEX Upgrade in view of ITER applications, Plasma Phys. Control. Fus. **49**, B341 (2007). https://doi.org/10.1088/0741-3335/49/12B/S31

[27] C. Tsironis et al., Electron-cyclotron wave scattering by edge density fluctuations in ITER, Phys. Plasmas **16**, 112510 (2009). https://doi.org/10.1063/1.3264105

[28] H. Weber et al., Scattering of diffracting beams of electron cyclotron waves by random density fluctuations in inhomogeneous plasmas, EPJ Web of Conf. **87**, 01002 (2015). https://doi.org/10.1051/epjconf/20158701002

[29] A. Köhn et al., Microwave beam broadening due to turbulent plasma density fluctuations within the limit of the Born approximation and beyond, Plasma Phys. Control. Fus. **60**, 075006 (2018). https://doi.org/10.1088/1361-6587/aac000

[30] O. Chellaï et al., Millimeter-wave beam scattering and induced broadening by plasma turbulence in the TCV tokamak, Nucl. Fusion **61**, 066011 (2021). https://doi.org/10.1088/1741-4326/abf43f

[31] C. C. Petty et al, Detailed measurements of the electron cyclotron current drive efficiency on DIII-D, Nucl. Fusion **42**, 1366 (2002). https://doi.org/10.1088/0029-5515/42/12/303